Per-antenna Power Minimization in Symbol-level Precoding for the Multi-beam Satellite Downlink

Danilo Spano[1*] Symeon Chatzinotas[1], Stefano Andrenacci[1], Jens Krause[2] and Björn Ottersten[1]

[1]*SnT - securityandtrust.lu, University of Luxembourg, 29 Avenue J.F. Kennedy, L-1855 Luxembourg*
[2]*SES, Chateau de Betzdorf, Luxembourg*

SUMMARY

This paper addresses the problem of multi-user interference in the forward downlink channel of a multi-beam satellite system. A symbol-level precoding scheme is considered, in order to exploit the multi-user interference and transform it into useful power at the receiver side, through a joint utilization of the data information and the channel state information. In this context, a per-antenna power minimization scheme is proposed, under Quality-of-Service constraints, for multi-level modulation schemes. The consideration of the power limitations individually for each transmitting RF chain is a central aspect of this work, and it allows to deal with systems using separate per-antenna amplifiers. Moreover, this feature is also particularly relevant for systems suffering non-linear effects of the channel. This is the case of satellite systems, where the non-linear amplifiers should be properly driven in order to reduce the detrimental saturation effect. In the proposed scheme, the transmitted signals are designed in order to reduce the power peaks, while guaranteeing some specific target signal-to-noise ratios at the receivers. Numerical results are presented in order to show the effectiveness of the proposed scheme, which is compared both to the state of the art in symbol-level precoding and to the conventional MMSE precoding approach.

1. INTRODUCTION

One of the biggest challenges in the current research on satellite communication (SatCom) systems is the need to break the existent throughput gridlock, in order to fulfill the ever-increasing demand for interactive services and multimedia content delivery. In particular, the throughput requirements for the next generation of SatCom systems are striving towards the terabit/s capacity [1–5]. In order to achieve this target, it is pivotal to find feasible technical solutions taking into account that the wireless spectrum is a scarce resource, which is getting more and more congested. The state of

---

*Correspondence to: SnT - securityandtrust.lu, University of Luxembourg, 29 Avenue J.F. Kennedy, L-1855 Luxembourg. E-mail: danilo.spano@uni.lu

the art in high throughput SatCom relies on multi-beam architectures, which exploit the spatial degrees of freedom offered by antenna arrays to aggressively reuse the available spectrum, thus realizing a space division multiple access (SDMA) scheme [6]. As a matter of fact, aggressive frequency reuse schemes are possible only if advanced signal processing techniques are developed, with the objective of handling the multi-user interference (MUI) arising in multi-beam systems and deteriorating their performance. Such signal processing techniques are commonly referred to as multi-user multiple-input multiple-output (MU-MIMO) and, in the satellite context, also as multi-beam joint processing. In this context, linear precoding (or beamforming) techniques have been a prolific recent area in the recent years, showing to be an effective way to manage the MUI while guaranteeing some specific service requirements [7–12]. The benefits of using precoding techniques for managing the interference at the gateway in SatCom are also considered in the most recent extensions of broadband multi-beam SatCom standards [13].

The conventional precoding approach exploits the knowledge of the channel state information (CSI) in order to design a precoder to be applied to the multiple data streams, thus mitigating the MUI. Since the precoder depends only on the CSI, it remains constant for a whole block of symbols whose length is related to the coherence time of the channel. Therefore, we can refer to this scheme as block-level precoding. The most relevant closed-form solutions for block-level precoding are the well known zero-forcing (ZF) precoding [14, 15] and minimum mean square error (MMSE) precoding [16, 17]. Over-the-air demonstrations for such schemes have been recently proposed for SatCom systems [18]. Beyond these closed-form schemes, a number of precoding strategies based on the numerical solution of optimization problems have been considered in the literature, which allow to optimize the system with respect to specific objectives. The optimal precoding algorithm for the minimization of the total transmit power, whilst guaranteeing some Quality-of-Service (QoS) targets at each user, was given in [10, 12], while the max-min fair problem under sum power constraints (SPC) was optimally solved in [11]. The latter strategy aims to maximize the minimum signal-to-interference-plus-noise ratio (SINR) amongst the users, in order to preserve the fairness of the system. The research work on block-level precoding was extended in [19] accounting for per-antenna power constraints (PACs), and in [20,21] considering generalized power constraints. Furthermore, the problem of block-level precoding in a multigroup multicast framework has been tackled in [22].

A different precoding strategy, considered more recently in the literature, is known as symbol-level precoding [23–28]. In this approach, the transmitted signals are designed based on the knowledge of both the CSI and the data information (DI), constituted by the symbols to be delivered to the users. Since the design exploits also the DI, the objective of symbol-level precoding is not to eliminate the interference, but rather to control it so to have a constructive interference effect at each user. The classification of the interference as constructive or destructive was given in [23], where a selective channel inversion scheme was proposed in order to eliminate the destructive interference. A more advanced symbol-level precoding scheme was proposed in [24], based on the rotation of the destructive interference, with the aim to transform it into useful power. Different optimization approaches have been proposed in the literature for symbol-level precoding. In [25] the sum-power minimization and the max-min fair problem were solved for M-PSK modulations. Furthermore, symbol-level precoding has been considered for multicast-based systems and for multi-level modulations, including also flexible schemes accounting an imperfect knowledge of

the CSI, as well as relaxed detection regions [27–29]. The potential of symbol-level precoding has been further explored by the authors in [30, 31], where the per-antenna power limitations of the transmitter are accounted on a symbol basis, for M-PSK modulation schemes.

Extending the work of [30, 31], this paper addresses the problem of per-antenna power minimization in symbol-level precoding accounting for multi-level modulation schemes. The consideration of the power limitations individually for each transmitting RF chain is a central aspect of this work, and is motivated by the practical implementation of most systems that rely on precoding. In fact, a common practice in multi-antenna systems is the use of individual per-antenna amplifiers, and this implies a lack of flexibility in sharing energy resources amongst the antennas of the transmitter. In spite of the possibility of using flexible amplifiers so to handle this issue, specific communication systems cannot afford this design. Typical per-antenna power limited systems can be found in multi-beam SatCom [32], where flexible on-board payloads are difficult to implement. In addition to this, the proposed per-antenna power minimization approach is also particularly relevant for systems with non-linear channels. This is the case of Satcom, where the non-linear effects are usually introduced by the on-board per-antenna traveling-wave-tube amplifiers (TWTAs), which result in a distortion on the transmitted waveforms [13, 33–35]. A typical solution to this problem in single-user links relies on predistortion techniques [33, 36, 37], but their extension to multi-beam systems relying on precoding is not straightforward, because of the mutual correlation between the data streams induced by the precoding schemes. About this, a joint predistortion algorithm for multi-beam systems is given in [38]. In this context, the proposed precoding strategy allows to design more robust signals to the non-linear effects. In particular, the symbol-level design allows to have a control on the instantaneous per-antenna transmit power, thus reducing the power peaks amongst the different antennas. In this direction, different symbol-level strategies devised for non-linear channels have been recently proposed in [39, 40], where however the objective is not the minimization of the per-antenna transmit power. Overall, the main contributions of this paper can be summarized as follows:

- A novel symbol-level precoding strategy is proposed, performing a per-antenna power minimization under QoS constraints, guaranteeing the required SINR to each user. Compared to the state of the art symbol-level techniques, this design allows the reduction of the power peaks among the different antennas, for each symbol slot, and therefore improves the robustness of the signals to the non-linear effects.
- First, the algorithm is formalized and solved for the case of single-level modulations (i.e., M-PSK). Then, the scheme is generalized for multi-level constellations.
- The performance of the proposed approach is assessed through simulations in a realistic SatCom scenario.

The remainder of the paper is organized as follows. In Section 2, the system and signals communication model is delineated. In Section 3, the symbol-level peak power minimization problem is proposed and solved. In Section 4, the proposed approach is validated through simulation results. Finally, in Section 5 conclusions are drawn.

Notation: We use upper-case and lower-case bold-faced letters to denote matrices and vectors, respectively. $(\cdot)^T$ denotes the transpose of $(\cdot)$. $|\cdot|$ and $\angle(\cdot)$ denote the amplitude and the phase of $(\cdot)$, respectively, while $\mathrm{Re}(\cdot)$ and $\mathrm{Im}(\cdot)$ are the real and imaginary parts of $(\cdot)$, and ι is used

to denote the imaginary unit. $\| \cdot \|$ and $\| \cdot \|_\infty$ represent the Euclidean norm and the l_∞ norm of $(\cdot)$, respectively. Moreover, $\mathrm{Pr}(\cdot)$ denotes the probability of an event, $\mathrm{diag}(\cdot)$ denotes a diagonal matrix whose diagonal entries are the elements of $(\cdot)$, and $\circ$ is used for denoting the element-wise Hadamard operations. Finally, $\unrhd$ is used as a generalized inequality for the optimization constraints, to be read as $\geq$ or as $=$ depending whether the constraint is referred to a boundary symbol or to an internal symbol of the constellation, respectively.

2. SYSTEM AND SIGNALS MODEL

We consider a multi-user (MU) multiple-input multiple-output (MIMO) satellite system, and we denote by K the number of antennas of the on-board transmitter. These antennas allow the generation of K independent beams through a parabolic reflector. Let us also assume that K single-antenna users are served in a specific instant, namely considering one user per beam[†]. We consider a general multi-level modulation, and we assume a channel vector $\boldsymbol{h}_j \in \mathbb{C}^{1 \times K}$ between the transmitting antennas and the j-th user. The received signal at the j-th user in the symbol slot n can be written as:

$$y_j[n] = \boldsymbol{h}_j \boldsymbol{x}[n] + z_j[n], \tag{1}$$

where $\boldsymbol{x}[n] \in \mathbb{C}^{K \times 1}$ represents the transmitted signal vector from the K transmit antennas, and $z_j[n]$ is a random variable distributed as $\mathcal{CN}(0, \sigma_z^2)$, modeling the zero mean Additive White Gaussian Noise (AWGN) measured at the j-th user's receiving antenna.

By collecting the received signals by all the users in a vector $\boldsymbol{y}[n] \in \mathbb{C}^{K \times 1}$, the above model can be rewritten in a compact form as:

$$\boldsymbol{y}[n] = \boldsymbol{H}\boldsymbol{x}[n] + \boldsymbol{z}[n], \tag{2}$$

where $\boldsymbol{H} = [\boldsymbol{h}_1^T \ldots \boldsymbol{h}_K^T]^T \in \mathbb{C}^{K \times K}$ represents the system channel matrix, and $\boldsymbol{z}[n] \in \mathbb{C}^{K \times 1}$ collects the AWGN components for all the users.

The transmitted signal vector $\boldsymbol{x}[n]$ is obtained as output of a precoding module, which takes as input the CSI, which is an estimate of $\boldsymbol{H}$, and the data information $\boldsymbol{d}[n] \in \mathbb{C}^{K \times 1}$, namely the data symbols to be conveyed to the users. The data symbols are assumed to be uncorrelated and taken from a constellation represented by the symbol set $\mathcal{D}$, having unit average power, i.e., $\mathbb{E}_\mathcal{D}[|d_j|^2] = 1$. In the transmission scheme we assume a framing structure including a preamble of pilot symbols. Such pilots are exploited by each user to estimate the related channel vector, and the resulting CSI is fed back to the gateway in order to be available for the precoding operation.

2.1. Multi-beam Channel Model

The complex matrix $\boldsymbol{H}$, modeling the multi-beam satellite channel, can be written as follows:

[†]This is reasonable if the systems resorts to a time-division multiplexing scheme, in order to serve all the users in each beam.

$$\boldsymbol{H} = \boldsymbol{L} \circ \boldsymbol{B} \circ \boldsymbol{\Phi}, \tag{3}$$

where $\boldsymbol{B} \in \mathbb{R}^{K \times K}$ models the gains related to the multi-beam satellite radiation pattern, $\boldsymbol{\Phi} \in \mathbb{C}^{K \times K}$ models the signal phase rotations induced by the on-board RF chains and by the propagation paths, while the matrix $\boldsymbol{L} \in \mathbb{R}^{K \times K}$ includes the link budget coefficient for each antenna-user pair.

The elements of $\boldsymbol{B}$ depend on the multi-beam radiation pattern at hand, and on the users position. Regarding the phase rotations, they are assumed independent for each antenna-user pair, so as to take into account the different propagation paths between the transmitter and the users, as well as the different on-board RF chains[‡]. Accordingly, the generic element of the matrix $\boldsymbol{\Phi}$ in (3) is modeled as $[\boldsymbol{\Phi}]_{jk} = e^{\iota \phi_{jk}}$, where ϕ_{jk} are independent random variables uniformly distributed in $[0, 2\pi) \; \forall j, k = 1, \ldots, K$.

Finally, considering the generic (j, k) element of the matrix $\boldsymbol{L}$, related to the link between the k-th beam's antenna and the j-th user's antenna, it will be given by:

$$[\boldsymbol{L}]_{jk} = \sqrt{G_{Rj}} \left(4\pi \frac{d_{jk}}{\lambda} \right)^{-1}, \tag{4}$$

with G_{Rj} being the j-th user's receiving antenna gain, d_{jk} being the distance between the j-th user and the the k-th beam's antenna, and λ the wavelength.

2.2. Non-linearities of the Satellite Channel

As anticipated, it should be taken into account how the system model introduced in (2) is actually degraded by the non-linear effects introduced by the on-board per-antenna TWTAs. To model such non-linear effects, we write in polar coordinates the input signal to the TWTA on the generic i-th RF chain of the transmitter as[§]:

$$x_i = r_i \exp(\iota \theta_i), \tag{5}$$

where r_i and θ_i are the amplitude and the phase of x_i, respectively. Then, the output signal of the TWTA can be written as:

$$\hat{x}_i = f_A(r_i) \exp(\iota f_P(r_i)) \exp(\iota \theta_i), \tag{6}$$

with $f_A(\cdot)$ and $f_P(\cdot)$ denoting the AM-AM and the AM-PM conversions, respectively. The resulting system model is shown in Fig. 1.

An analytical description of the amplitude and phase distortion induced by the TWTAs is given in [41], with the well known Saleh model. Further, different numerical models for the input-output characteristics of the amplifiers are provided in [13, 35]. We take as a reference the common non-linearized TWTA model of [35], whose normalized amplitude-to-amplitude (AM-AM) and amplitude-to-phase (AM-PM) characteristics are shown in Fig. 2. The characteristics clearly show the saturation effect and the introduced phase shifts.

[‡]In particular, we take into account phase shifts introduced on each RF chain due to on-board payload imperfections and/or different on-board propagation paths. This justifies the assumption of independent phases among the different RF chains. Nonetheless, the main conclusions of this work are still valid if a different model for $\boldsymbol{\Phi}$ is considered.

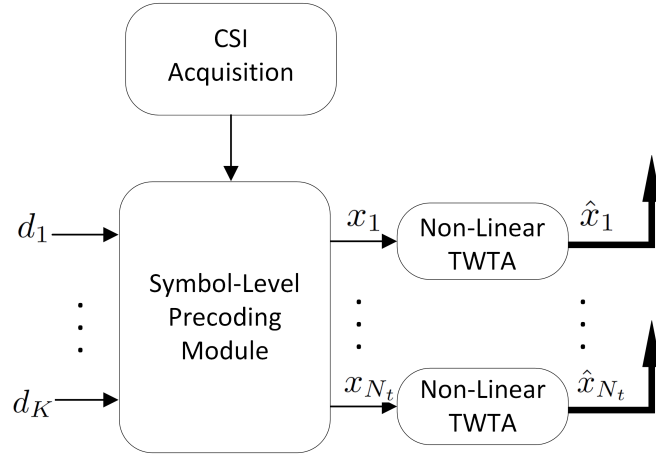[§]In order to ease the notation, hereafter the time index n is omitted in formulas.

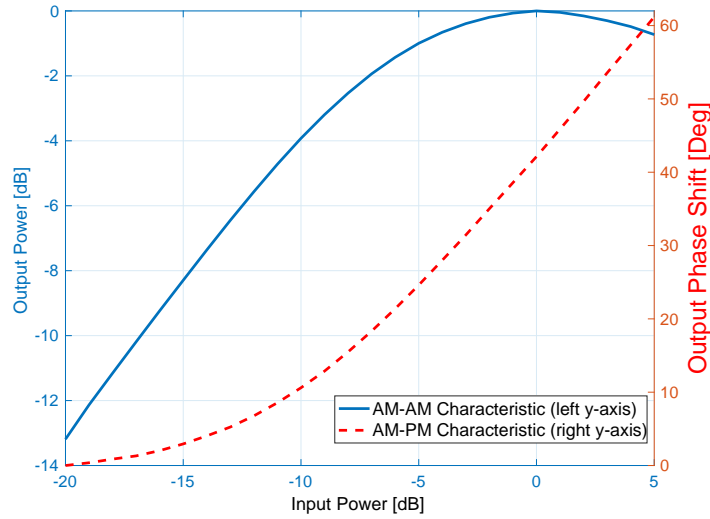Figure 1. Block scheme of the transmitter relying on symbol-level precoding, for a generic symbol slot.

Figure 2. Normalized AM-AM and AM-PM characteristics of the on-board TWTAs (non-linearized model) [35].

The on-board TWTAs need to be operated as close as possible to saturation, to efficiently exploit the scarce available power. As a consequence, the need of controlling the power level of the transmitted waveforms is crucial in order to reduce the detrimental effect of the non-linearities of the satellite channel. Moreover, in systems using separate per-antenna TWTAs, a different phase distortion is induced over the various data streams, because of the different instantaneous power carried out by the symbols of each stream. This additional issue, which we refer to as *differential phase shift*, is particularly relevant when precoding is applied, since the power imbalances between the transmitting antennas are usually not controlled. Therefore, a reduced power variation of the precoded waveforms is needed also in the space dimension, i.e., between the different antennas. In this direction, besides accounting for the per-beam power limitations, the proposed symbol-level precoding approach allows to reduce the power imbalances between the different transmitting antennas, thus improving the robustness of the waveforms to the channel non-linearities.

3. SYMBOL-LEVEL PRECODING FOR PEAK POWER MINIMIZATION

The aim is to design the transmitted vector $\boldsymbol{x}$, based on the CSI and the DI, assuring that the received signal lies in the detection region of the desired symbol, for each user. This way, the interfering signals are forced to constructively contribute to the useful received power, in line with the definition of constructive interference provided in [25]. In this context, the objective is to minimize the per-antenna transmit power under per-beam QoS constraints, for each symbol slot. Such minimization can be seen as the minimization of the peak power between the antennas, therefore we will refer to the proposed scheme as symbol-level precoding for peak power minimization (SL-PPM). We start by addressing the problem for M-PSK modulations, in the fashion of [30, 31]. Then, the problem will be extended to the general case of multi-level modulation schemes.

3.1. SL-PPM for Single-level Modulations

Focusing on the case of single-level modulations, i.e., M-PSK, the SL-PPM optimization problem can be written as follows:

$$
\begin{aligned}
\boldsymbol{x}(\boldsymbol{d}, \boldsymbol{H}, \boldsymbol{\gamma}) = \arg \min_{\boldsymbol{x}} \max_{i=1,\ldots,K} & \quad \{|x_i|^2\} \\
& \text{subject to} \\
\mathcal{C}1: \quad |\boldsymbol{h}_j \boldsymbol{x}|^2 & \geq \gamma_j \sigma_z^2, \ j = 1, \ldots, K, \\
\mathcal{C}2: \quad \angle \boldsymbol{h}_j \boldsymbol{x} & = \angle d_j, \ j = 1, \ldots, K,
\end{aligned}
\tag{7}
$$

where γ_j is the target SINR that should be granted for the j-th user, and $\boldsymbol{\gamma} = [\gamma_1 \ldots \gamma_K]^T \in \mathbb{C}^{K \times 1}$ stacks the target SINR for all the users. The set of constraints $\mathcal{C}1$ represents a QoS constraint for each user, while the set of constraints $\mathcal{C}2$ represents the constructive interference condition, guaranteeing that each user receives the desired data symbol with the correct phase. In order to write the optimization problem in a more tractable form, we carry out the following steps, following the method of [42].

First of all, by defining $\alpha_j = \tan(\angle d_j) \ \forall j = 1, \ldots, K$, the constraint $\mathcal{C}2$ in (7) can be rewritten, by applying the tangent operator[¶], as

$$
\frac{\text{Im}(\boldsymbol{h}_j \boldsymbol{x})}{\text{Re}(\boldsymbol{h}_j \boldsymbol{x})} = \alpha_j, \ j = 1, \ldots, K.
\tag{8}
$$

However, since the tangent is not a one-to-one function, the following conditions should be added, in order to ensure that the received symbol and the intended one lie in the same quadrant:

$$
\begin{aligned}
\text{Re}(d_j) \text{Re}(\boldsymbol{h}_j \boldsymbol{x}) &\geq 0, \ j = 1, \ldots, K, \\
\text{Im}(d_j) \text{Im}(\boldsymbol{h}_j \boldsymbol{x}) &\geq 0, \ j = 1, \ldots, K.
\end{aligned}
\tag{9}
$$

Secondly, the QoS constraint $\mathcal{C}1$ in the problem (7) can be reformulated referring to the amplitude levels of the in-phase and quadrature components of the corresponding symbols, as follows:

[¶]This does not apply for data symbols laying on the imaginary axis, since the tangent is not defined in such case. Although this case can be easily handled, it is not considered herein, since we can always assume a phase offset preventing this situation.

$$|\operatorname{Re}(\boldsymbol{h}_j\boldsymbol{x})| \geq \sigma_z\sqrt{\gamma_j}|\operatorname{Re}(d_j)|, \ j = 1,\ldots,K,$$
$$|\operatorname{Im}(\boldsymbol{h}_j\boldsymbol{x})| \geq \sigma_z\sqrt{\gamma_j}|\operatorname{Im}(d_j)|, \ j = 1,\ldots,K, \quad (10)$$

where the absolute value is necessary for accounting negative components. By multiplying both the members of the above equations by $\operatorname{Re}(d_j)$ and $\operatorname{Im}(d_j)$ respectively, and by taking into account the conditions in (9), the above constraints become:

$$\operatorname{Re}(d_j)\operatorname{Re}(\boldsymbol{h}_j\boldsymbol{x}) \geq \sigma_z\sqrt{\gamma_j}\operatorname{Re}^2(d_j), \ j = 1,\ldots,K,$$
$$\operatorname{Im}(d_j)\operatorname{Im}(\boldsymbol{h}_j\boldsymbol{x}) \geq \sigma_z\sqrt{\gamma_j}\operatorname{Im}^2(d_j), \ j = 1,\ldots,K. \quad (11)$$

With these new constraints, and resorting to the concept of l_∞-norm, the problem (7) can be rewritten as:

$$\boldsymbol{x}(\boldsymbol{d},\boldsymbol{H},\boldsymbol{\gamma}) = \ \arg\min_{\boldsymbol{x}} \quad ||\boldsymbol{x}||_\infty$$

subject to

$$\mathcal{C}1: \quad \operatorname{Re}(d_j)\operatorname{Re}(\boldsymbol{h}_j\boldsymbol{x}) \geq \sigma_z\sqrt{\gamma_j}\operatorname{Re}^2(d_j), \ j = 1,\ldots,K, \quad (12)$$
$$\mathcal{C}2: \quad \operatorname{Im}(d_j)\operatorname{Im}(\boldsymbol{h}_j\boldsymbol{x}) \geq \sigma_z\sqrt{\gamma_j}\operatorname{Im}^2(d_j), \ j = 1,\ldots,K,$$
$$\mathcal{C}3: \quad \frac{\operatorname{Im}(\boldsymbol{h}_j\boldsymbol{x})}{\operatorname{Re}(\boldsymbol{h}_j\boldsymbol{x})} = \alpha_j, \ j = 1,\ldots,K,$$

and, in a more compact form, as follows:

$$\boldsymbol{x}(\boldsymbol{d},\boldsymbol{H},\boldsymbol{\gamma}) = \arg\min_{\boldsymbol{x}} \quad ||\boldsymbol{x}||_\infty$$

subject to

$$\mathcal{C}1: \quad \operatorname{Re}(\boldsymbol{D})\operatorname{Re}(\boldsymbol{H}\boldsymbol{x}) \geq \boldsymbol{\beta_r} \quad (13)$$
$$\mathcal{C}2: \quad \operatorname{Im}(\boldsymbol{D})\operatorname{Im}(\boldsymbol{H}\boldsymbol{x}) \geq \boldsymbol{\beta_i}$$
$$\mathcal{C}3: \quad \boldsymbol{A}\operatorname{Re}(\boldsymbol{H}\boldsymbol{x}) - \operatorname{Im}(\boldsymbol{H}\boldsymbol{x}) = \boldsymbol{0},$$

where $\boldsymbol{D} = \operatorname{diag}(\boldsymbol{d})$, $\boldsymbol{A} = \operatorname{diag}(\alpha_1,\ldots,\alpha_K)$, $\boldsymbol{\beta_r} = \sigma_z\sqrt{\boldsymbol{\gamma}}\circ\operatorname{Re}(\boldsymbol{d})^{\circ 2}$, $\boldsymbol{\beta_i} = \sigma_z\sqrt{\boldsymbol{\gamma}}\circ\operatorname{Im}(\boldsymbol{d})^{\circ 2}$.

The problem (13) can be written as a second-order cone programming (SOCP) [43] in the stacked variable $\tilde{\boldsymbol{x}} = [\operatorname{Re}(\boldsymbol{x})^T, \operatorname{Im}(\boldsymbol{x})^T]^T \in \mathbb{R}^{2K\times 1}$. To this end, the objective function should be written as:

$$||\boldsymbol{x}||_\infty = \max_{i=1,\ldots,K}\{|x_i|\} = \max_{i=1,\ldots,K}||\boldsymbol{E}_i\tilde{\boldsymbol{x}}||, \quad (14)$$

where $\boldsymbol{E}_i \in \mathbb{R}^{2\times 2K}$ is a matrix used for selecting $\operatorname{Re}(x_i)$ and $\operatorname{Im}(x_i)$ in the stacked vector $\tilde{\boldsymbol{x}}$ and, $\forall i = 1,\ldots,K$, is in turn defined as:

$$\boldsymbol{E}_i = \begin{bmatrix} \boldsymbol{e}_i & \boldsymbol{0}_K^T \\ \boldsymbol{0}_K^T & \boldsymbol{e}_i \end{bmatrix}, \quad (15)$$

with $\boldsymbol{e}_i$ being the i-th row of an identity matrix with size K, and $\boldsymbol{0}_K$ being the all zero entries vector in $\mathbb{R}^{K\times 1}$.

By defining the $\boldsymbol{H_1} = [\operatorname{Re}(\boldsymbol{H}), -\operatorname{Im}(\boldsymbol{H})]$ and $\boldsymbol{H_2} = [\operatorname{Im}(\boldsymbol{H}), \operatorname{Re}(\boldsymbol{H})]$, the problem (13) becomes:

$$\tilde{x}(d, H, \gamma) = \arg \min_{\tilde{x}} \max_{i=1,\ldots,K} \quad ||E_i \tilde{x}||$$

$$\text{subject to}$$

$$\mathcal{C}1: \quad \text{Re}(D)H_1 \tilde{x} \geq \beta_r,$$
$$\mathcal{C}2: \quad \text{Im}(D)H_2 \tilde{x} \geq \beta_i, \tag{16}$$
$$\mathcal{C}3: \quad (AH_1 - H_2)\tilde{x} = 0.$$

Finally, by introducing a slack variable r, the SL-PPM problem can be formulated as a SOCP as follows:

$$\tilde{x}(d, H, \gamma) = \arg \min_{r, \tilde{x}} \quad r$$

$$\text{subject to}$$

$$\mathcal{C}1: \quad ||E_i \tilde{x}|| \leq r, \ i = 1, \ldots, K,$$
$$\mathcal{C}2: \quad \text{Re}(D)H_1 \tilde{x} \geq \beta_r \tag{17}$$
$$\mathcal{C}3: \quad \text{Im}(D)H_2 \tilde{x} \geq \beta_i$$
$$\mathcal{C}4: \quad (AH_1 - H_2)\tilde{x} = 0.$$

This optimization problem can be efficiently solved using standard convex optimization tools. For this work, we rely on the CVX tool [43].

3.2. SL-PPM for Multi-level Modulations

We consider now a generalized version of the SL-PPM problem (7), assuming a multi-level modulation scheme for the DI. In this case, while imposing the constructive interference constraints, the symbol-level optimization strategy will have to take into account whether the DI symbols at hand are internal points of the constellation or border ones. Accordingly, the optimization problem can be generalized as follows:

$$x(d, H, \gamma) = \arg \min_{x} \max_{i=1,\ldots,K} \quad \{|x_i|^2\}$$

$$\text{subject to}$$

$$\mathcal{C}1: \quad |h_j x|^2 \unrhd \kappa_j^2 \gamma_j \sigma_z^2, \ j = 1, \ldots, K, \tag{18}$$
$$\mathcal{C}2: \quad \angle h_j x = \angle d_j, \ j = 1, \ldots, K,$$

where $\kappa_j = |d_j|/\sqrt{\mathbb{E}_{\mathcal{D}}[|d_j|^2]}$ is a magnitude scaling factor for the symbol d_j, which allows to account the different amplitudes of the symbols in the multi-level constellation $\mathcal{D}$. The assumption to have symbols with unit average power implies that $\kappa_j = |d_j|$. As anticipated, the notation $\unrhd$ is used as a generalized inequality which allows to unify different constraints for the internal points of the constellation, for which we impose an equality, and for the border ones, for which an inequality is considered (generalized inequalities related to the different detection regions can be also found in [26, 29]).

Analogously to the previous case, the constraints of (18) can be reformulated referring to the in-phase and quadrature components of the corresponding symbols. In particular, the constraint $\mathcal{C}1$ can be written as:

$$|\operatorname{Re}(\boldsymbol{h}_j \boldsymbol{x})| \trianglerighteq \sigma_z \sqrt{\gamma_j} |\operatorname{Re}(d_j)|, \; j = 1, \ldots, K,$$
$$|\operatorname{Im}(\boldsymbol{h}_j \boldsymbol{x})| \trianglerighteq \sigma_z \sqrt{\gamma_j} |\operatorname{Im}(d_j)|, \; j = 1, \ldots, K. \tag{19}$$

Applying the same procedure as before, the problem can be reformulated as a SOCP, as follows:

$$\tilde{\boldsymbol{x}}(\boldsymbol{d}, \boldsymbol{H}, \boldsymbol{\gamma}) = \arg \min_{r, \tilde{\boldsymbol{x}}} \quad r$$

$$\text{subject to}$$

$$\mathcal{C}1: \quad ||\boldsymbol{E}_i \tilde{\boldsymbol{x}}|| \leq r, \; i = 1, \ldots, K,$$
$$\mathcal{C}2: \quad \operatorname{Re}(\boldsymbol{D}) \boldsymbol{H_1} \tilde{\boldsymbol{x}} \trianglerighteq \boldsymbol{\beta_r} \tag{20}$$
$$\mathcal{C}3: \quad \operatorname{Im}(\boldsymbol{D}) \boldsymbol{H_2} \tilde{\boldsymbol{x}} \trianglerighteq \boldsymbol{\beta_i}$$
$$\mathcal{C}4: \quad (\boldsymbol{A} \boldsymbol{H_1} - \boldsymbol{H_2}) \tilde{\boldsymbol{x}} = \boldsymbol{0},$$

and this final formulation can be efficiently solved resorting to standard convex optimization tools, such as CVX [43].

4. NUMERICAL RESULTS

In this section some numerical results are presented, in order to evaluate the performance of the proposed approach. The performance is evaluated both in terms of transmit power (peak and average) and in terms of achieved SINR at the receivers[||]. The numerical analysis is based on a 71-beam antenna satellite system ($K = 71$) operating in the Ka band with carrier frequency of 19.5 GHz and user bandwidth of 500 MHz. A single polarization is assumed, along with a full frequency reuse scheme. The satellite is located on the Geostationary Earth Orbit at longitude of $30°E$. The beam centers are located in the positions marked in Fig. 3, and the users are assumed positioned in the centers of the respective beams, unless specified otherwise. The receiving antennas are assumed having a diameter of 0.6 m, while the noise temperature is set to 240 K. Moreover, a 16-APSK modulation scheme is assumed for the DI, while a perfect knowledge of the CSI is assumed at the transmitter. Further, for simplicity the considered channel does not account for fading[**].

4.1. Benchmark schemes

First, we consider as benchmark the symbol-level precoding scheme of [25, 26, 29], which performs sum power minimization (SL-SPM), comparing the achieved performance in terms of peak and average transmit power. This benchmark allows to assess the proposed scheme in terms of instantaneous power distribution among the antennas. It should be highlighted that the power distribution is evaluated before the non-linear TWTAs on the transmit RF chains, as a more uniform distribution would improve the robustness of the waveforms to the non-linear effects, and

---

[||]In this work we have chosen the SINR as figure of merit, since a performance evaluation in terms of achieved rate is not straightforward under a finite alphabet assumption. An evaluation of the achievable information rate for symbol-level precoding is left for the future work.

[**]However, the gains of the proposed approach hold if a flat fading effect is modeled (see [40]). Besides, recent extensions of symbol-level precoding (see [44]) allow to handle the inter-symbol interference, thus frequency-selective fading channels are foreseen to be tackled in the future work.
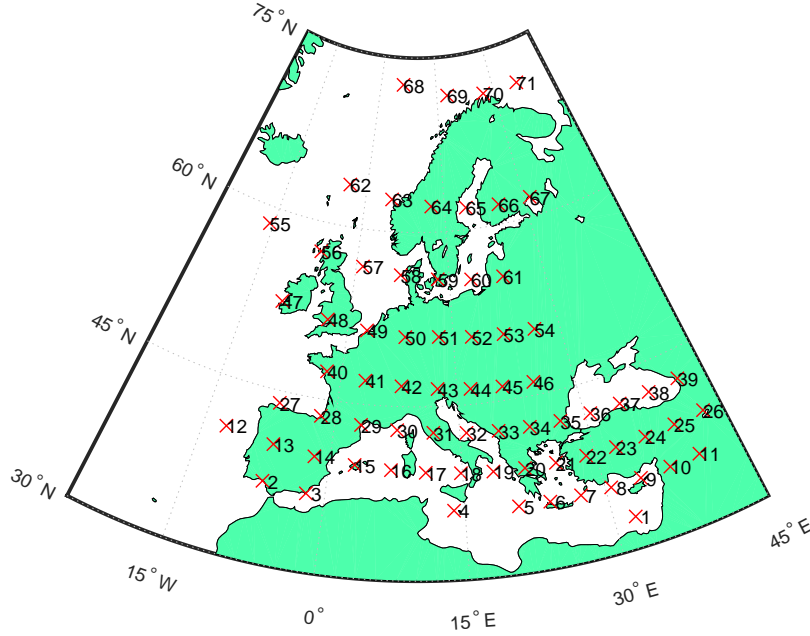
Figure 3. Coverage region of the considered satellite systems; the numbered marks represent the beam centers.

in particular to the problem of differential phase shift. For the sake of completeness, we provide in the following a formulation for the SL-SPM optimization problem:

$$
\begin{aligned}
\boldsymbol{x}(\boldsymbol{d}, \boldsymbol{H}, \boldsymbol{\gamma}) = \arg \min_{\boldsymbol{x}} \quad & \|\boldsymbol{x}\|^2 \\
& \text{subject to} \\
\mathcal{C}1: \quad & |\boldsymbol{h}_j \boldsymbol{x}|^2 \unrhd \kappa_j^2 \gamma_j \sigma_z^2, \ j = 1, \ldots, K, \\
\mathcal{C}2: \quad & \angle \boldsymbol{h}_j \boldsymbol{x} = \angle d_j, \ j = 1, \ldots, K.
\end{aligned}
\tag{21}
$$

Afterwards, the proposed approach is compared with the conventional MMSE precoding scheme [16, 17] in terms of attained SINR at the receivers, so as to observe the constructive interference effect of the symbol-level precoding strategy[††]. A comparison in terms of per-beam transmit power is also presented. For the sake of completeness, we shall mention that in the MMSE case the transmit vector $\boldsymbol{x}$ is calculated by weighting the original symbols through a precoding matrix $\boldsymbol{W}$, as $\boldsymbol{x} = \boldsymbol{W} \boldsymbol{d}$, and that the precoding matrix can be written as $\boldsymbol{W} = \boldsymbol{H}^H (\boldsymbol{H} \boldsymbol{H}^H + \eta \boldsymbol{I})^{-1}$. In turn, η represents a regularization parameter inversely proportional to the signal-to-noise ratio. The power constraints of the system at hand can be accounted by accordingly rescaling the precoding matrix $\boldsymbol{W}$.

[††]While symbol-level precoding has already been compared to conventional optimization-based schemes in [25, 26], herein we choose as benchmark a closed-form block-level scheme such as MMSE, which has been widely investigated in the SatCom literature. It should be stressed that the main goal of this block-level benchmark is to assess the SINR gain due to the constructive interference effect of the symbol-level strategy, and that this assessment is focused on per-antenna power limited SatCom systems without accounting for non-linearities. A full chain analysis directly focused on non-linear systems and accounting for the oversampled waveforms can be found in [40].

4.2. Comparison with the SL-SPM scheme

Herein, we present some numerical results comparing the proposed approach with the SL-SPM scheme formulated in (21), in terms of peak and average transmit power. The symbol-level average power transmitted by each antenna is defined as $P_{\text{av}} = \frac{||\boldsymbol{x}||^2}{K}$, whilst the symbol-level peak power among the antennas will be $P_{\text{peak}} = ||\boldsymbol{x}||^2_{\infty}$. By taking an average of such quantities over a large number of symbol slots, we obtain the frame-level average power and peak power, which are used as performance metric hereafter.

Fig. 4 shows the introduced power metrics, in dBW, as a function of the target SINR, assumed the same for all the users for the sake of simplicity. The result shows how the required transmit power increases with the target SINR, and how the proposed SL-PPM approach attains better performance in terms of peak power with respect to the SL-SPM scheme. On the other hand, the proposed approach requires a higher average transmit power. Overall, the SL-PPM approach allows to reduce the instantaneous power peaks amongst the different beams at the expense of a higher average transmit power, achieving a more uniform instantaneous power distribution amongst the antennas. As already mentioned, this is particularly important with respect to the problem of non-linear TWTAs. For completeness, we present in Fig. 5 an analogous result obtained by considering the users' locations uniformly distributed within the respective beams, and by averaging over several realizations for the users' distribution. The result shows how, in this general case, the gains of the proposed approach in terms of reduced peak power are even higher with respect to the case of users located in the center of the beams. It can also be noticed how, given the target SINR, the required transmit power is considerably higher (both for the proposed scheme and for the benchmark) with respect to the scenario with central users, because of the higher interference experienced.

In order to better illustrate the performance of the proposed strategy in terms of instantaneous power distribution, we show in Fig. 6 the instantaneous power utilization for each of the 71 beams, for a fixed symbol slot. The SINR target is set at 10 dB. Such representation clearly shows how, sacrificing some average power, the proposed approach leads to a more uniform distribution of the power between the antennas, resulting in a lower peak power.

4.3. Comparison with the MMSE Precoding

Hereafter we focus on the comparison between symbol-level precoding, in particular the proposed SL-PPM scheme, and MMSE precoding. The evaluation is done in terms of achieved average and per-beam SINR, as well as in terms of per-beam transmit power.

Fig. 7 shows the achieved SINR, averaged between the different beams, as a function of the available per-beam power. Such power represents a per-beam constraint on the power consumption, intended as the transmit power averaged over the temporal dimension. It is interesting to notice how the SL-PPM scheme outperforms MMSE precoding, and how the gap between the two approaches increases with the per-beam power. This result can be explained by considering that the symbol-level precoding exploits the constructive interference effect, which allows to have a considerable increase in the SINR at the receivers. Moreover, it shall be highlighted how a raise in the transmit power determines also a raise in the interference level among the beams: while this is a harmful factor in the MMSE case, it actually allows a better interference exploitation in the SL-PPM strategy, and this justifies the dependence of the achieved SINR gain on the power. We also show in Fig. 8 the
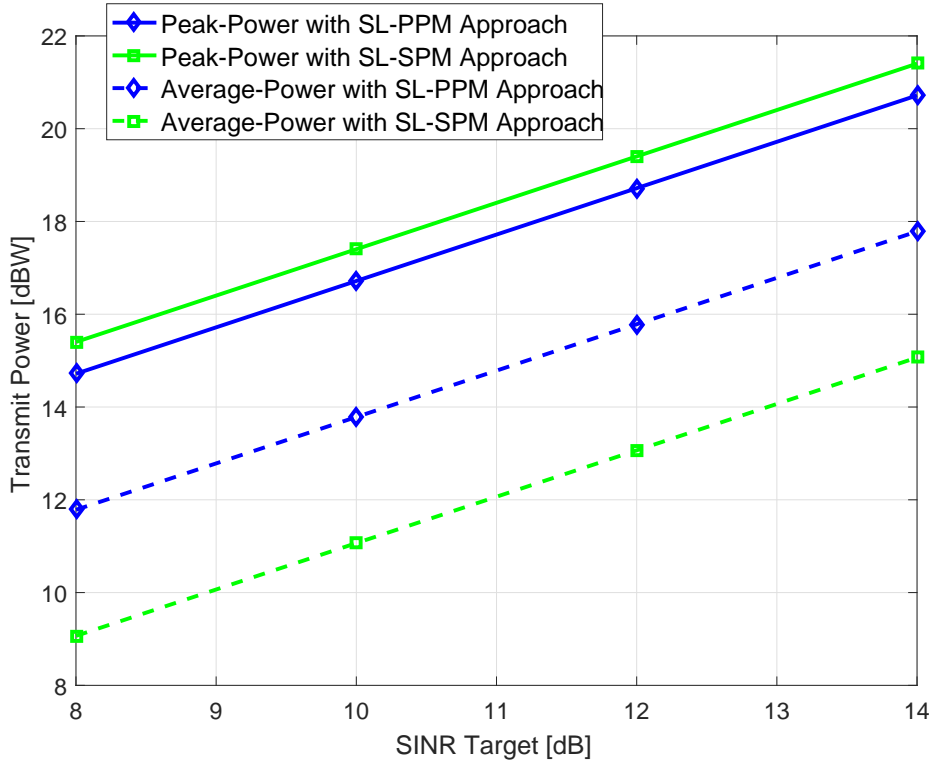
Figure 4. Frame-level transmit power in dBW vs. SINR target in dB.

SINR comparison in the case of users uniformly distributed within the respective beams, averaging over several realizations for the users' locations. In this general case, it can be seen how the higher interference level due to the different users' location determines a further increase in the gap between the symbol-level scheme and the block-level one.

In Fig. 9 the distribution of the achieved SINR among the different beams is illustrated, when a per-beam available power of 16 dBW is considered. From this result, it is apparent how the SL-PPM approach outperforms MMSE for each beam, and not only in average.

In the comparative analysis at hand, further insights can be given by observing how the power consumption varies among the different beams. Considering again a per-beam available power of 16 dBW, Fig. 10 displays the transmit power (averaged over time) for each beam, in dBW, both for SL-PPM and MMSE. Interestingly, the symbol-level approach exploits more efficiently the available power than the MMSE scheme, where the power consumption results less balanced. This fact can be identified as an additional reason of the improved SINR performance of the proposed scheme.

For the sake of completeness, we also compare the distribution of the peak power among the different beams for the proposed approach and the MMSE scheme. In particular, considering again a per-beam available average power of 16 dBW, we show in Fig. 11 the empirical evaluation of the cumulative distribution function (CDF) of the instantaneous peak power obtained with the two approaches. The CDF of the peak power P_{peak} is a function of a variable P_0 defined as the probability of P_{peak} being less than P_0, i.e., $\text{CDF}_{P_{\text{peak}}}(P_0) = \text{Pr}(P_{\text{peak}} < P_0)$. The result highlights how the peak power of the proposed scheme is always below the one of the MMSE precoder, with a gap of
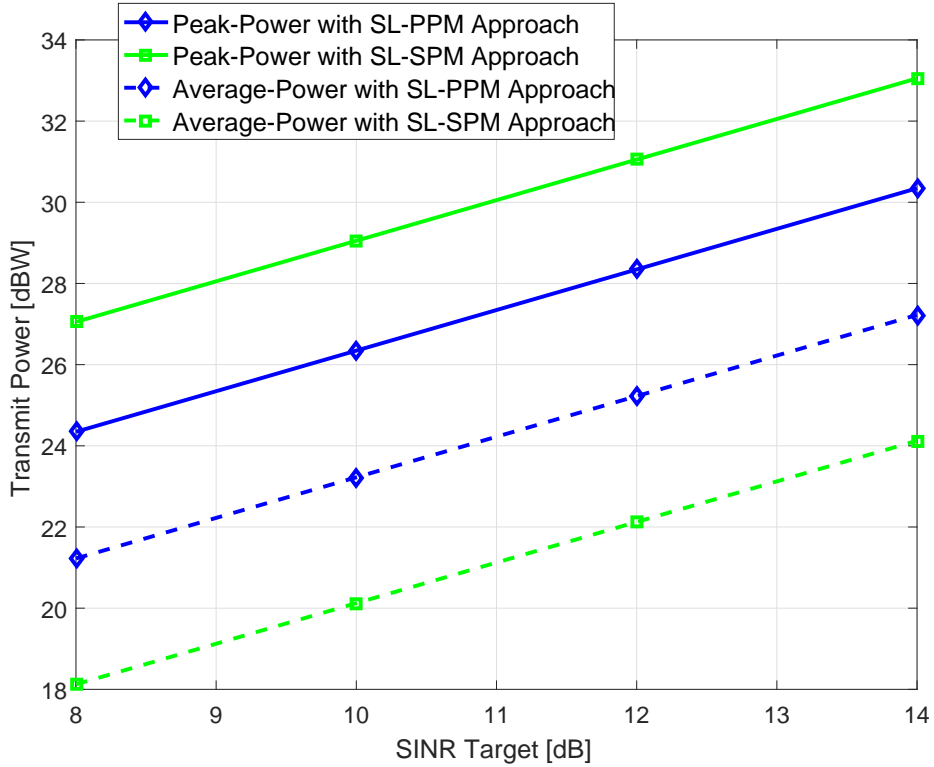
Figure 5. Frame-level transmit power in dBW vs. SINR target in dB, for uniformly distributed users in the beams.

approximately 1.5 dB in the median values. To better illustrate this effect, we consider in Fig. 12 the instantaneous power distribution among the different beams for a fixed symbol slot. It is visible how, also compared to the MMSE precoding, the proposed approach determines a more uniform distribution of the instantaneous power, making the transmitted signal more robust to the non-linear effects of the TWTAs.

As mentioned above, all the presented results are obtained under the assumption of perfect CSI knowledge at the transmitter. However, it is well known from the literature that the available CSI usually has some level of uncertainty, due to errors in the channel estimation and to the non ideal feedback link. Accordingly, it should be kept in mind that the performance of precoding in a practical scenario would be degraded with respect to the considered ideal case. In particular, the achieved SINR values presented in Figs. 7-9 would be reduced both for the proposed SL-PPM scheme and for the MMSE approach. While a quantitative analysis of this effect is out of the scope of this contribution, the results herein presented provide a performance benchmark and reveal the most suitable scenarios where precoding can be further developed accounting for non ideal conditions. However, we stress that the gains of the proposed scheme in terms of peak power reduction would hold even with an imperfect CSI, because of the applied optimization strategy. Further considerations on channel errors in the context of symbol-level precoding can be found in [28], where a robust power minimization scheme is proposed.
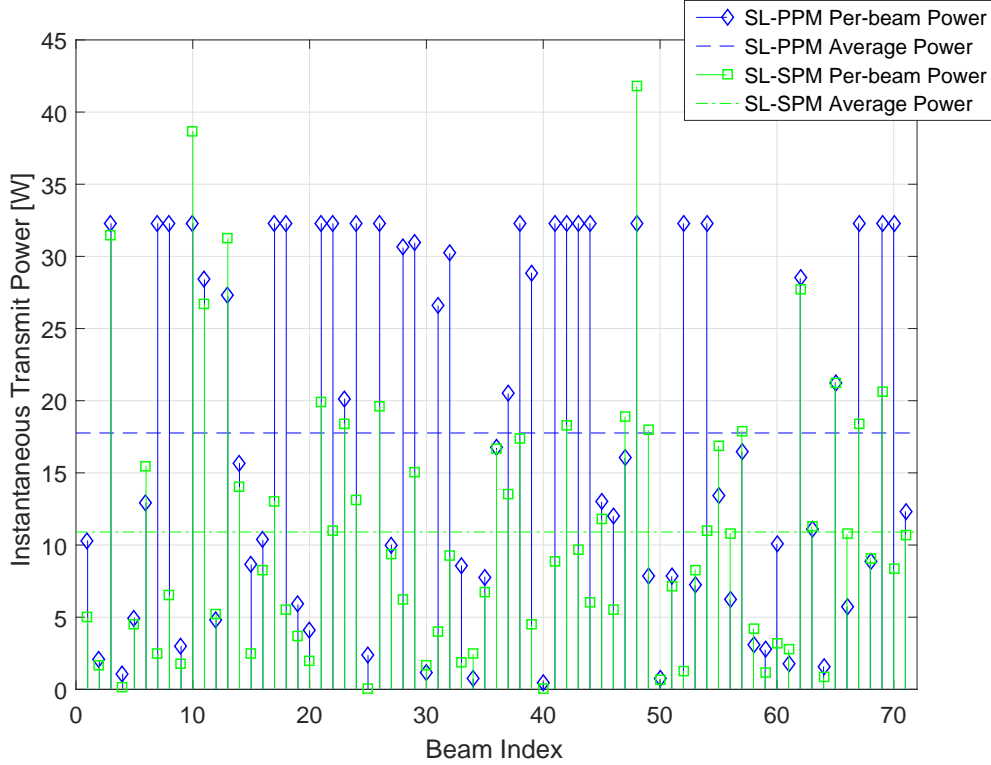
Figure 6. Instantaneous per-beam transmit power, in W, for a certain DI vector.

4.4. Discussion on Complexity

We conclude this section by discussing the complexity of the proposed approach. In this regard, a first fundamental remark to make is that symbol-level precoding schemes require the calculation of the transmit signal vector x for each symbol slot, as outlined in Fig. 1. This implies that the symbol-level precoding algorithm needs to be applied for every symbol slot, thus its switching rate coincides with the baudrate. On the other hand, in block-level precoding schemes, the precoder remains constant for a whole block of symbols whose length is related to the coherence time of the channel. Accordingly, symbol-level precoding schemes are inherently more complex than the block level ones, as discussed in [25].

Herein, we focus on symbol-level schemes, and specifically we compare the proposed SL-PPM approach (20) with the SL-SPM one (21) in terms of complexity. Since the proposed optimization problems are tackled resorting to numerical convex optimization tools [43], analytical expressions for the complexity are hard to derive. Therefore, we evaluate the complexity based on the average running time of the algorithms over the same machine. The complexity assessment, shown in Fig. 13, has been carried out as a function of the system size K, i.e., the number of transmit antennas as well as of users, by averaging over several random channel matrices. As expected, the proposed SL-PPM scheme turns out to be more complex than the SL-SPM one. Interestingly, the complexity gap between the two approaches tends to increase with K. It shall be stressed that the provided running time values are used solely as a comparative numerical assessment of the complexity, while they should not be read as the actual processing time of the precoding schemes in a real world
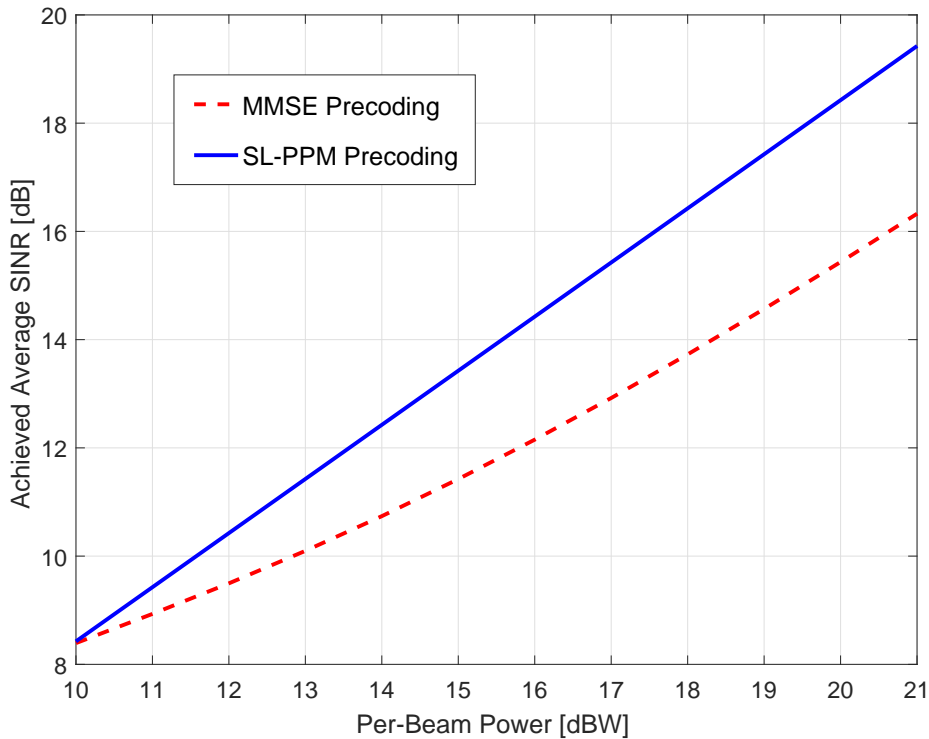
Figure 7. Average SINR, in dB, vs. available per-beam power.

implementation. In fact, the actual processing time would depend on the specific algorithms chosen to solve the problems (20)-(21) and on their hardware implementation. The processing time is a critical parameter towards the practical utilization of the schemes, and in real systems it should be much lower than the round trip time, in order not to make the CSI outdated. A thorough study in this regard falls out of the scope of this paper, however it is part of the ongoing work [45, 46].

5. CONCLUSIONS

In this work a novel technique for symbol-level precoding has been proposed, taking into account the per-antenna power limitations that arise typically in satellite systems. In particular, the problem of minimization of the peak power amongst the transmitting antenna, under QoS constraints, is formulated and solved, in order to have a more uniform distribution of the transmitted power with respect to the state of the art symbol-level techniques. The optimization scheme has been derived first for the case of single-level modulations, and then extended to the general case of multi-level modulations. The considered peak power minimization design is suitable for systems corrupted by non-linear effects, such as satellite ones, where the power peaks reduction, and more in general the control on the transmitted power, implies relevant benefits. The performance of the proposed scheme is assessed through numerical results, in comparison to the symbol-level sum power minimization scheme and to the MMSE precoding. In the former case, it is shown how the proposed approach
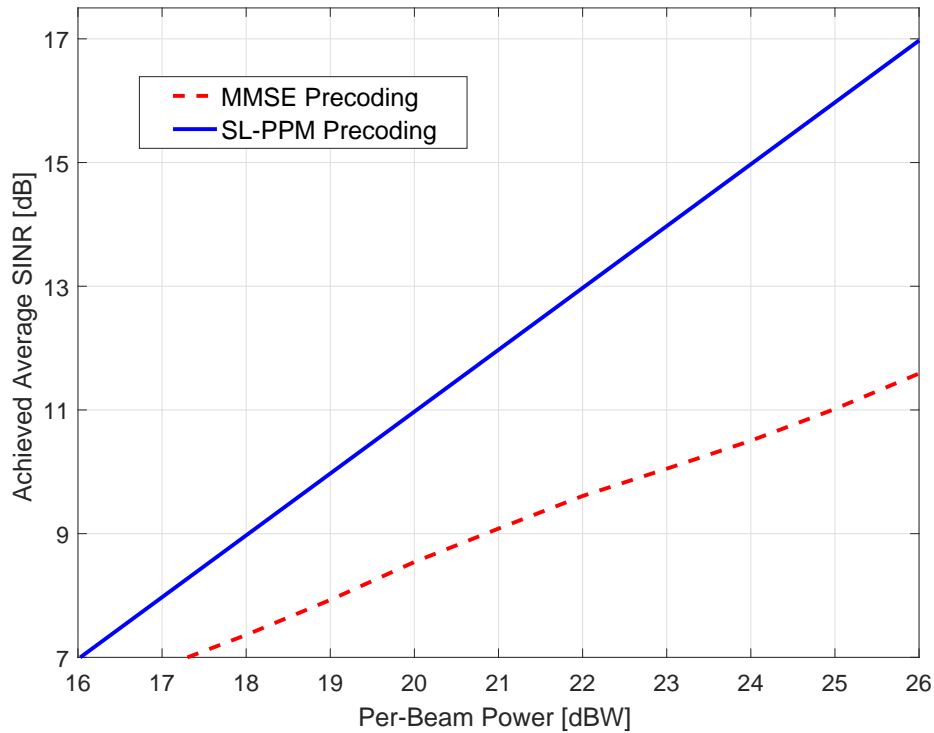
Figure 8. Average SINR, in dB, vs. available per-beam power, for uniformly distributed users in the beams.

gains in terms of a reduced transmitted peak power across the antennas, at the expense of a higher required average power. In the latter case, the SINR gains of symbol-level precoding over the conventional MMSE are demonstrated, together with the improved behavior in terms of power peaks among the antennas.

References

1. Gayrard JD. Terabit satellite: Myth or reality? *Advances in Satellite and Space Communications, 2009. SPACOMM 2009. First International Conference on*, 2009; 1–6, doi:10.1109/SPACOMM.2009.17.
2. Mignolo D, Re E, Ginesi A, Alamanac AB, Angeletti P, Harverson M. Approaching terabit/s satellite capacity: A system analysis. *Proc. Ka Broadband Conf.*, 2011.
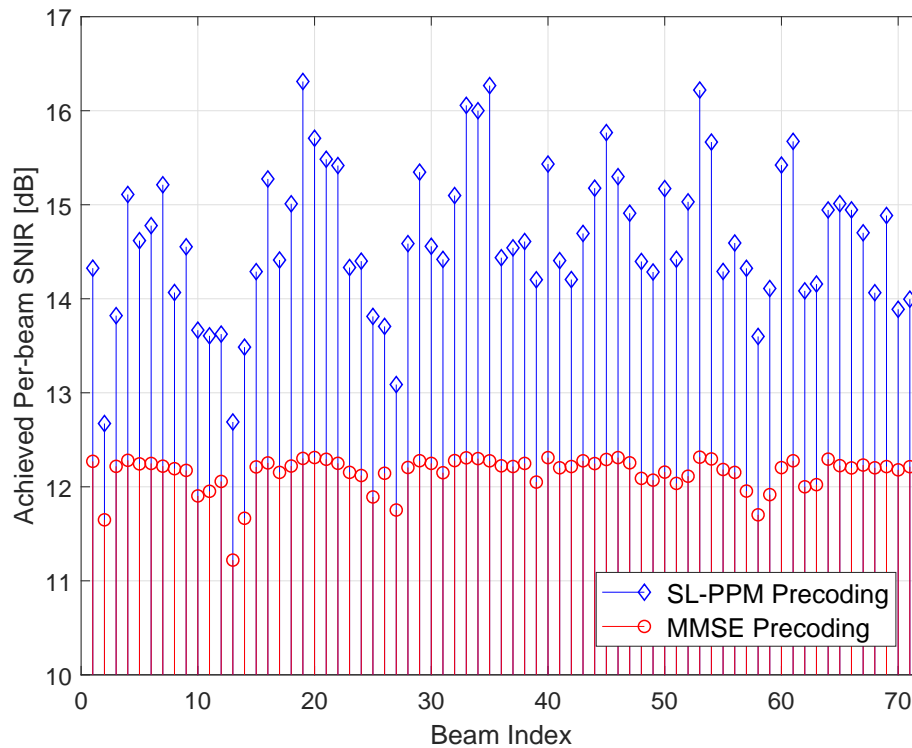
Figure 9. Achieved per-beam SINR, in dB, for an available per-beam power of 16 dBW.

3. Evans B, Thompson P. Key issues and technologies for a terabit/s satellite. *28th AIAA International Communications Satellite Systems Conference (ICSSC-2010)*, 2010.

4. Thompson P, Evans B, Castenet L, Bousquet M, Mathiopoulos T. Concepts and technologies for a terabit/s satellite. *SPACOMM 2011, The Third International Conference on Advances in Satellite and Space Communications*, 2011; 12–19.

5. Vidal O, Verelst G, Lacan J, Alberty E, Radzik J, Bousquet M. Next generation high throughput satellite system. *Satellite Telecommunications (ESTEL), 2012 IEEE First AESS European Conference on*, 2012; 1–7, doi: 10.1109/ESTEL.2012.6400146.

6. Roy R, Ottersten B. Spatial division multiple access wireless communication systems May 1996; URL `https://www.google.com/patents/US5515378`, US Patent 5,515,378.

7. Liu YF, Dai YH, Luo ZQ. Coordinated beamforming for MISO interference channel: Complexity analysis and efficient algorithms. *IEEE Transactions on Signal Processing* 2011; **59**(3):1142–1157.

8. Björnson E, Bengtsson M, Ottersten B. Optimal multiuser transmit beamforming: A difficult problem with a simple solution structure [lecture notes]. *IEEE Signal Processing Magazine* July 2014; **31**(4):142–148, doi: 10.1109/MSP.2014.2312183.

9. Gershman AB, Sidiropoulos ND, Shahbazpanahi S, Bengtsson M, Ottersten B. Convex optimization-based beamforming. *IEEE Signal Processing Magazine* May 2010; **27**(3):62–75, doi:10.1109/MSP.2010.936015.

10. Bengtsson M, Ottersten B. Optimal and suboptimal transmit beamforming. *Handbook of Antennas in Wireless Communications*. CRC Press, 2001.

11. Schubert M, Boche H. Solution of the multiuser downlink beamforming problem with individual SINR constraints. *IEEE Transactions on Vehicular Technology* Jan 2004; **53**(1):18–28, doi:10.1109/TVT.2003.819629.

12. Bengtsson M, Ottersten B. Optimal downlink beamforming using semidefinite optimization. *Proc. of Annual Allert. Conf. on Commun. Control and Computing*, vol. 37, Citeseer, 1999; 987–996.

13. ETSI EN 302 307-2. Digital video broadcasting (DVB); second generation framing structure, channel coding and modulation systems for broadcasting, interactive services, news gathering and other broadband satellite applications; part 2: DVB-S2 extensions (DVB-S2X).
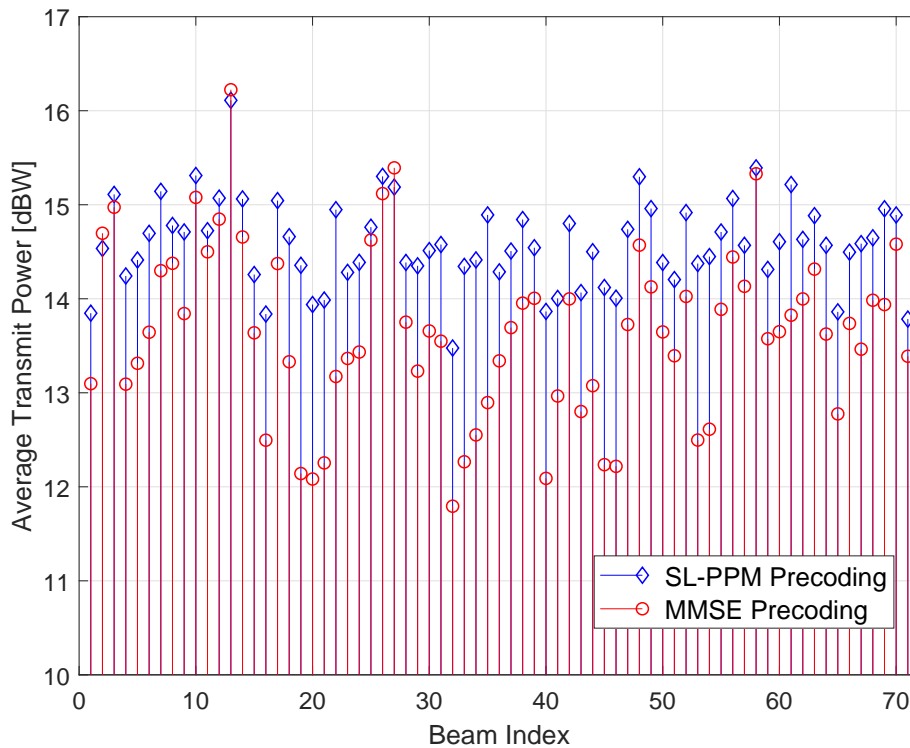
Figure 10. Transmit power distribution among the beams, for an available per-beam power of 16 dBW.

14. Yoo T, Goldsmith A. Optimality of zero-forcing beamforming with multiuser diversity. *IEEE International Conference on Communications (ICC 2005)*, vol. 1, 2005; 542–546, doi:10.1109/ICC.2005.1494410.
15. Yoo T, Goldsmith A. Capacity and power allocation for fading MIMO channels with channel estimation error May 2006; **52**(5):2203–2214.
16. Choi RLU, Murch R. New transmit schemes and simplified receivers for MIMO wireless communication systems 2003; **2**(6):1217–1230.
17. Peel C, Hochwald B, Swindlehurst A. A vector-perturbation technique for near-capacity multiantenna multiuser communication - part i: channel inversion and regularization 2005; **53**(1):195–202.
18. Hamet B, Rohde C, Bhave P, Liddell A. Over-the-air field trials of linear precoding for multi-spot-beam satellite systems. *22nd Ka and Broadband Communications Conference*, 2016.
19. Yu W, Lan T. Transmitter optimization for the multi-antenna downlink with per-antenna power constraints. *IEEE Transactions on Signal Processing* June 2007; **55**(6):2646–2660, doi:10.1109/TSP.2006.890905.
20. Dartmann G, Gong X, Afzal W, Ascheid G. On the duality of the max min beamforming problem with per-antenna and per-antenna-array power constraints. *IEEE Transactions on Vehicular Technology* Feb 2013; **62**(2):606–619, doi:10.1109/TVT.2012.2222946.
21. Zheng G, Chatzinotas S, Ottersten B. Generic optimization of linear precoding in multibeam satellite systems. *IEEE Transactions on Wireless Communications* June 2012; **11**(6):2308–2320, doi:10.1109/TWC.2012.040412.111629.
22. Christopoulos D, Chatzinotas S, Ottersten B. Weighted fair multicast multigroup beamforming under per-antenna power constraints. *IEEE Transactions on Signal Processing* Oct 2014; **62**(19):5132–5142, doi:10.1109/TSP.2014.2345340.
23. Masouros C, Alsusa E. Dynamic linear precoding for the exploitation of known interference in MIMO broadcast systems. *IEEE Transactions on Wireless Communications* March 2009; **8**(3):1396–1404, doi:10.1109/TWC.2009.080053.
24. Masouros C. Correlation rotation linear precoding for MIMO broadcast communications. *IEEE Transactions on Signal Processing* Jan 2011; **59**(1):252–262.
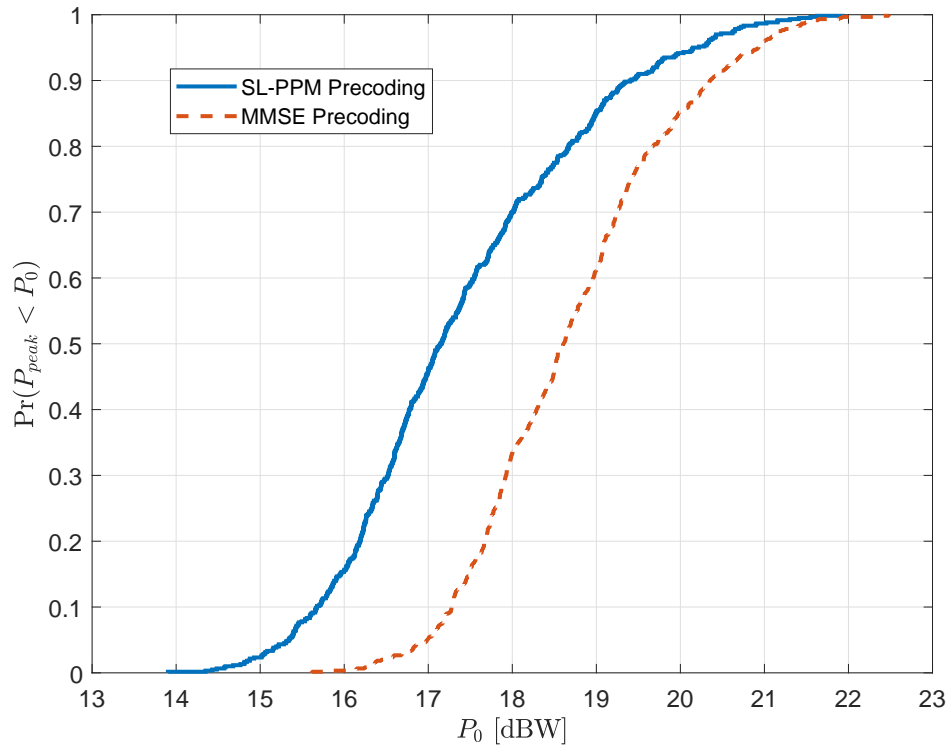
Figure 11. CDF of the peak power among the beams.

25. Alodeh M, Chatzinotas S, Ottersten B. Constructive multiuser interference in symbol level precoding for the MISO downlink channel. *IEEE Transactions on Signal Processing* May 2015; **63**(9):2239–2252, doi:10.1109/TSP.2015. 2404302.

26. Alodeh M, Chatzinotas S, Ottersten B. Symbol-level multiuser MISO precoding for multi-level adaptive modulation. *IEEE Transactions on Wireless Communications* Aug 2017; **16**(8):5511–5524, doi:10.1109/TWC. 2017.2712604.

27. Alodeh M, Chatzinotas S, Ottersten B. Energy-efficient symbol-level precoding in multiuser MISO based on relaxed detection region. *IEEE Transactions on Wireless Communications* May 2016; **15**(5):3755–3767, doi: 10.1109/TWC.2016.2528243.

28. Masouros C, Zheng G. Exploiting known interference as green signal power for downlink beamforming optimization. *IEEE Transactions on Signal Processing* July 2015; **63**(14):3628–3640, doi:10.1109/TSP.2015. 2430839.

29. Alodeh M, Chatzinotas S, Ottersten B. Constructive interference through symbol level precoding for multi-level modulation. *2015 IEEE Global Communications Conference (GLOBECOM)*, 2015; 1–6, doi:10.1109/GLOCOM. 2014.7417066.

30. Spano D, Alodeh M, Chatzinotas S, Ottersten B. Per-antenna power minimization in symbol-level precoding. *2016 IEEE Global Communications Conference (GLOBECOM)*, 2016; 1–6, doi:10.1109/GLOCOM.2016.7842126.

31. Spano D, Chatzinotas S, Krause J, Ottersten B. Symbol-level precoding with per-antenna power constraints for the multi-beam satellite downlink. *2016 8th Advanced Satellite Multimedia Systems Conference and the 14th Signal Processing for Space Communications Workshop (ASMS/SPSC)*, 2016; 1–8, doi:10.1109/ASMS-SPSC. 2016.7601542.

32. Christopoulos D, Arapoglou PD, Chatzinotas S, Ottersten B. Linear precoding in multibeam satcoms: Practical constraints. *31st AIAA International Communications Satellite Systems Conference (ICSSC)*, Florence, IT, 2013.

33. Casini E, Gaudenzi RD, Ginesi A. DVB-S2 modem algorithms design and performance over typical satellite channels. *International Journal of Sat. Comm. and Netw.* 2004; **22**(3):281–318, doi:10.1002/sat.791. URL http://dx.doi.org/10.1002/sat.791.
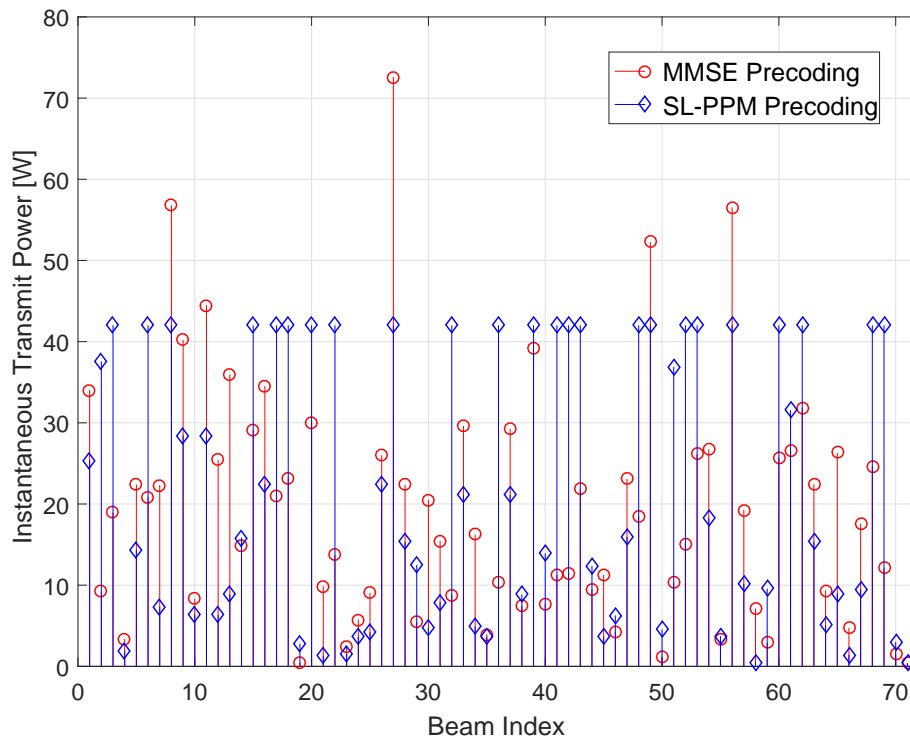
Figure 12. Instantaneous per-beam transmit power, in W, for a certain symbol vector.

34. Spano D, Christopoulos D, Andrenacci S, Chatzinotas S, Krause J, Ottersten B. Total degradation analysis of precoded signals onto non-linear satellite channels. *21st Ka and Broadband Communications Conference*, 2015.

35. ETSI EN 302 307-1. Digital video broadcasting (DVB); second generation framing structure, channel coding and modulation systems for broadcasting, interactive services, news gathering and other broadband satellite applications; part 1: DVB-S2.

36. Karam G, Sari H. A data predistortion technique with memory for QAM radio systems. *IEEE Transactions on Communications* 1991; **39**(2):336–344, doi:10.1109/26.76471.

37. Piazza R, Shankar MRB, Ottersten B. Data predistortion for multicarrier satellite channels based on direct learning. *IEEE Transactions on Signal Processing* Nov 2014; **62**(22):5868–5880, doi:10.1109/TSP.2014.2358958.

38. Mengali A, Shankar B, Ottersten B. Joint predistortion and PAPR reduction in multibeam satellite systems. *IEEE International Conference on Communications (ICC 2016)*, Kuala Lumpur, Malaysia, 2016.

39. Spano D, Alodeh M, Chatzinotas S, Krause J, Ottersten B. Spatial PAPR reduction in symbol-level precoding for the multi-beam satellite downlink. *2017 IEEE 18th International Workshop on Signal Processing Advances in Wireless Communications (SPAWC)*, 2017. URL `http://hdl.handle.net/10993/31224`.

40. Spano D, Alodeh M, Chatzinotas S, Ottersten B. Symbol-level precoding for the nonlinear multiuser MISO downlink channel. *IEEE Transactions on Signal Processing* March 2018; **66**(5):1331–1345, doi:10.1109/TSP.2017. 2781647.

41. Saleh AAM. Frequency-independent and frequency-dependent nonlinear models of TWT amplifiers. *IEEE Transactions on Communications* November 1981; **29**(11):1715–1720, doi:10.1109/TCOM.1981.1094911.

42. Kalantari A, Soltanalian M, Maleki S, Chatzinotas S, Ottersten B. Directional modulation via symbol-level precoding: A way to enhance security. *IEEE Journal of Selected Topics in Signal Processing* Dec 2016; **10**(8):1478–1493, doi:10.1109/JSTSP.2016.2600521.

43. Boyd S, Vandenberghe L. *Convex optimization*. Cambridge Univ. Press, 2004.

44. Spano D, Alodeh M, Chatzinotas S, Ottersten B. Faster-than-Nyquist signaling through spatio-temporal symbol-level precoding for the multiuser MISO downlink channel. *IEEE Transactions on Wireless Communications* 2018; URL `http://hdl.handle.net/10993/35040`, submitted.
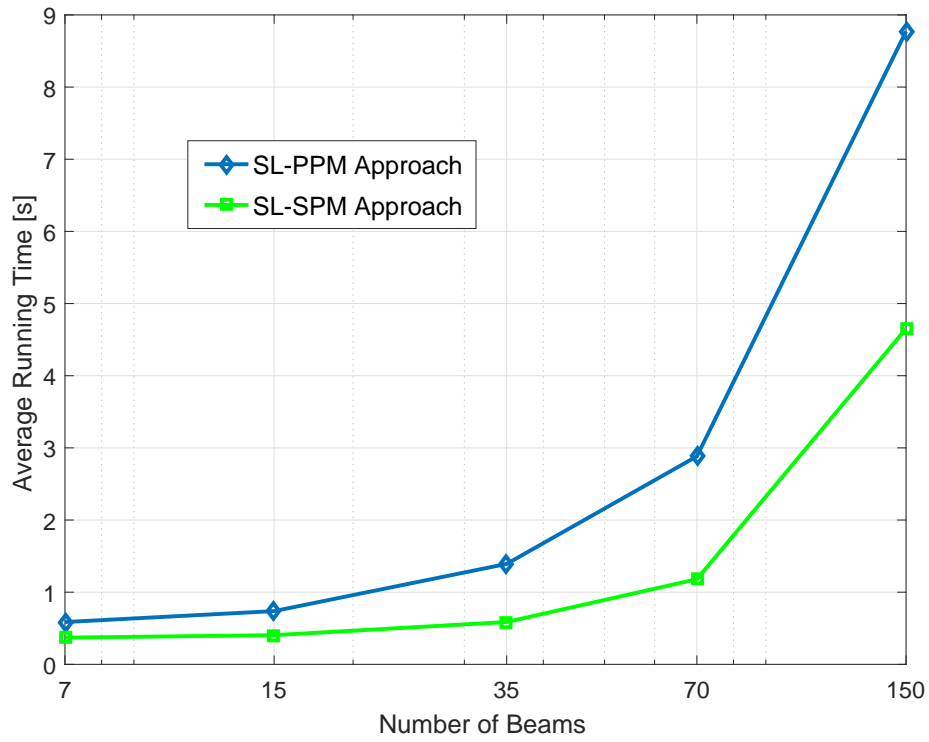
Figure 13. Average running time of the SL-SPM and SL-PPM algorithms, in s, versus K.

45. Krivochiza J, Kalantari A, Chatzinotas S, Ottersten B. Low complexity symbol-level design for linear precoding systems. *Symposium on Information Theory and Signal Processing in the Benelux*, 2017.
46. Duncan J, Krivochiza J, Chatzinotas S, Andrenacci S, Ottersten B. Computationally efficient symbol-level precoding communications demonstrator. *IEEE International Symposium on Personal, Indoor and Mobile Radio Communications, International Workshop on Efficiency, PIMRC 2017*, 2017.